npj Flexible Electronics

https://doi.org/10.1038/s41528-025-00500-w

Article in Press

Optical wireless data transfer through skin for implantable biomedical electronics

Received: 28 July 2025

Accepted: 11 November 2025

Cite this article as: Hong, C., Jung, D., Lee, T. *et al.* Optical wireless data transfer through skin for implantable biomedical electronics. *npj Flex Electron* (2025). https://doi.org/10.1038/s41528-025-00500-w

Changeui Hong, Dongwuk Jung, Taeyeon Lee & Jongho Lee

Optical Wireless Data Transfer Through Skin for Implantable Biomedical Electronics

Changeui Hong[1], Dongwuk Jung[1], Taeyeon Lee[1], and Jongho Lee[1*]

[1]Department of Mechanical and Robotics Engineering, Gwangju Institute of Science and Technology (GIST), Buk-gu, Gwangju 61005, Republic of Korea

[*]To whom correspondence should be address. E-mail: jong@gist.ac.kr

Abstract

As the global population ages, the demand for implantable medical electronic devices for physiological monitoring and functional support continues to grow. In such systems, wireless data exchange is essential for device control and real-time physiological data acquisition. While coil-based methods are widely used, the method may pose challenges such as electromagnetic interference, or unwanted induced currents in diverse clinical environments. Here, we introduce a soft, flexible optical wireless communication system capable of reliable, real-time data exchange through biological tissues without the need for antenna coils. Microscale light-emitting diodes (LEDs) and photodetector (PD), microfabricated and integrated into flexible platforms, enable wireless data transmission via light modulation through biological skin, in a relatively small form factor. *In vivo* experiments validate wireless bi-directional data transfer with integrated physiological sensors, demonstrating on-demand, real-time monitoring of signals such as electrocardiogram and body temperature. This approach offers a promising pathway toward safer, miniaturized wireless implantable electronics.

Introduction

As the human body ages or faces disease, various functions from organs can weaken or fail abruptly[1-3]. To support and restore these functions, a wide range of implantable electronic medical devices, such as pacemakers[4,5], nerve stimulators[6,7], artificial retina[8,9], and cochlear[10,11] have been developed with an aim to extend lifespan and improve quality of life significantly. While these devices are traditionally composed of rigid and bulky structures, recent advances in flexible electronics have enabled the development of soft, thin and flexible implants that provide higher mechanical compatibility with biological tissues, reducing stress and the risk of damage. Categories of flexible electronic implants include cardiac bioelectronics, designed to monitor and electrically regulate heart activity[4,5,12-14], neural interfaces, which enable high-resolution brain signal recording and stimulation[7,14-17], and sensory prostheses, which substitute lost sensory functions by stimulation[8,9,11,18-22]. Many of these flexible systems pursue reliable bio-signal acquisition or organ stimulation in fully implantable forms.

For the fully implanted devices to function effectively without transcutaneous wires, reliable wireless data exchange through live tissues is essential for real-time signal acquisition and device control. A widely adopted technology is inductive coupling, which utilizes two coils to induce an electrical current from a primary coil to a secondary coil via magnetic fields[23-25]. This method has been widely implemented in implantable electronics, including wireless power transfer, which enables stable energy delivery to operate functions of implants[26-28], wireless communication, which allows reliable data exchange between external device and implantable device[29-31], and electrical stimulation, which activates physiological functions without battery[5,14,32], due to its simplicity, ease of fabrication in flexible forms, and lower power consumption[33-35] compared to other wireless methods such as BLE, Bluetooth, and ultrasound communication[36]. While convenient, however, challenges persist. For example, coil alignment over deformable biological tissues can be challenging for patients. Moreover, the coil-based method may generate electromagnetic interference (EMI) or unwanted induced currents (eddy currents), potentially causing malfunctions or image artifacts in various medical diagnostic and therapeutic environments such as during MRI (Magnetic Resonance Imaging).

These potential issues in implantable devices can be relieved by using different communication media such as light whose frequency range (visual: 400−790 THz) is much different than the frequencies used in traditional medical devices (e.g., MRI scanners at ~20

ARTICLE IN PRESS

MHz −300 MHz). Despite its advantages, the application of optical wireless communication in implantable medical devices remains relatively unexplored. Recent studies have demonstrated convenient methods that enable optically acquiring physiological parameters such as glucose concentration, pH level, or temperature by detecting and differentiating the brightness of implanted LEDs with a photodetector or an external camera[37,38]. Other efforts have adopted more standard optical data transfer using commercially available infrared (IR) LEDs and IR receiver modules to collect bio-signals to the external devices[39,40]. While these early demonstrations showcase the feasibility of the approach, many critical factors such as design (e.g., small, thin and flexible), function capabilities (e.g., external control), and environmental considerations (e.g., tissue thickness and alignment) should be evaluated and addressed to be reliably integrated and used in electronic medical implants as interactive and programmable platforms for biomedical applications.

In this study, we present optical wireless communication with miniaturized bi-directional implantable devices that enable interactive device control and data acquisition through biological tissues using light, eliminating the need for antenna coils and thereby avoiding potential EMI or unwanted eddy currents[41]. The device footprint can be also minimized, as both the optical transmitter (light-emitting diodes, LEDs) and receiver (photodetector, PD) are microfabricated at the submillimeter scale using conventional photolithography. We systematically characterize communication performance depending on distance, alignment between the optical components, and the optical properties of biological tissues (i.e., skin). The feasibility of the method is demonstrated *in vivo* using live mouse models, where microscale optical devices integrated with implantable flexible sensors and a wearable patch enable bi-directional optical wireless data exchange, including real-time signal acquisition and device control, highlighting its potential uses for various biomedical applications.

Results

Optical wireless data transfer through biological tissues

A conceptual illustration of optical wireless communication from a body appears in **Figure 1a**. An implanted device, equipped with light-emitting diodes (LEDs), generates light signal that can penetrate biological tissues as in Figure 1b, enabling secure transmission of physiological data out of a body. For example, the LEDs under a pig skin can signal out of the skin as the on and off states can be observed in bright or dark environments as shown with the optical images in Figure 1c.

As the light generated in a body is visible out of the body, optical wireless data transfer can be realized by different optical modulation strategies. The simplest one is to make use of light intensity by controlling the input voltage to the LEDs as in Figure 1d. An advantage is that the strength of the signal can be differentiated with a naked eye, for example, when reading a body temperature. Another way of data transfer is by controlling light-emitting frequencies in a body and reading the frequencies out of a skin, for example, a low frequency (1 Hz) to note low temperature (<37 ℃), and a high frequency (10 Hz) to note high temperature (≥40 ℃) as in Figure 1e.

The more versatile way of the optical wireless data transfer is by delivering digital signals through biological tissues after encoding data in a body into binary signals, sending the signals through tissues by modulating LEDs on and off as illustrated in Figure 1f. An alphabet 'A' can be encoded to binary data "01000001", transmitted through a biological tissue with the corresponding modulated light (binary signals), and captured by an external photodetector (PD). The delivered binary signals can be decoded back into the alphabet "A", enabling optical wireless communication of any characters through biological tissues. Additional details are provided in SI (Supplementary Fig. 1). The illustrations and optical images in Figure 1g,h show the preliminary experimental setup of optical wireless data transfer through an isolated pig skin (thickness, *t*: ~3 mm) placed between the optical signal transmitter (LEDs, Figure 1g) and the optical signal receiver (photodetector, PD, Figure 1h). The encoded binary signals in voltage applied to the transmitter (LEDs, 10000010, "A", upper in Figure 1i) are clearly delivered to the photodetector (PD, 10000010, "A", lower in Figure 1i) through the pig skin. Although the optical signal voltage at the receiver was measured in a dark environment to ensure accurate acquisition, the signal was still detectable even under indoor light condition (~5000 lux). More details are in SI (Supplementary Fig. 2). The optical transmitter implanted in the live mouse model can be used to wirelessly deliver internal biological information to the attached optical receiver out of the body as shown in Figure 1j.

Design and performance characteristics of the implantable optical wireless device

The optical wireless device is fabricated to have both of the custom-made ultra-thin optical transmitter (LEDs) and receiver (PD) as a transceiver, in addition to electrocardiogram (ECG) electrodes as one of vital sensors, in a flexible form as illustrated in **Figure 2a**. The ultra-thin microLEDs (thickness: ~4 μm, 2 × 2 array, each size: 250 × 250 μm^2, AlGaInP) and PD (thickness: ~4 μm, size: 700 × 560 μm^2) was transfer-printed on a flexible polyimide (PI) film to face out of a body for data transfer while the ECG electrodes were deposited to face in a body for convenient measurement. The whole device is insulated and encapsulated by a PI layer (polyimide) and a soft silicone elastomer (10:1 polydimethylsiloxane, PDMS). More details of the fabrication process are provided in the Experimental section and SI (Supplementary Fig. 3). The fabricated implantable device is flexible enough to be bent around a glass rod with a radius of 9 mm as shown in Figure 2b. The magnified view of the fabricated microLEDs and PD are also shown in Figure 2c.

The optical and electrical characteristics of the integrated transceiver were evaluated to quantify the performances. Figure 2d shows the electroluminescence (EL) spectrum of the LEDs (red line, peak ~670 nm) and the external quantum efficiency (EQE) spectrum of the PD (blue line). Optical transmittance (blue line) through an isolated pig skin (thickness, *t*: ~3 mm) whose compositions and optical properties are similar to human skin[42-44], is also shown in Figure 2e. About 20% of the LEDs light can penetrate through the pig skin (*t* = ~3 mm). The current-voltage characteristics(I–V) of the LEDs in Figure 2f indicate the turn-on voltage of 2.13 V (forward current: 1 mA). The PD generates photocurrent of 79.3 μA at zero bias under red light illumination (wavelength: ~670 nm, optical power: ~0.28 mW) as shown with the I–V characteristics in Figure 2g.

Robustness of the optical wireless data transfer depends on distance and lateral alignment between the transmitter (LEDs) and receiver (PD). As the distance (*d*) increases from 0 to 50 mm, the measured signals (Figure 2h,i) by the PD reduces down to 45 mV, which is still enough for wireless communication. The lateral misalignment (*a*) also adversely affects the measured signal strength as in Figure 2j,k. With an increased misalignment upto 25 mm, the measured signals reduce down to 24 mV, which is still sufficient for wireless communication. The distance and alignment was controlled with a single-axis micro-stage. More details are provided in SI (Supplementary Fig. 4).

Although biological tissues attenuate optical signals, optical wireless data transfer can be done through a skin thickness of ~3 mm as shown with the experimental results without and with an isolated pig skin between the transmitter and receiver (Figure 2l-o). Average human skin thickness is around 1–3 mm[45]. With a vertical setup of the transmitter and receiver (distance, *d*: 3 mm) without a skin (Figure 2l), the transmitted binary signals (1010101) are received clearly (Figure 2m). With an isolated pig skin (thickness, *t*: 3 mm) inserted between the transmitter and receiver (Figure 2n) the received binary signals are clear too (Figure 2o). The optical image in Figure 2p shows that illuminated light penetrates through a biological tissue. Further evaluation with different skin thicknesses indicates that optical wireless data transfer through a relatively thick skin upto 9 mm can be done (detected signal: 30 mV, Figure 2q). Moreover, additional results on lateral misalignment with a biological tissue are provided in SI (Supplementary Fig. 5).

One of the advantages of the approach through biological tissues is that the fundamental frequency of light is in hundreds THz (visual light: 400–790 THz), way above those of other communication such as inductive coupling (125 kHz–13.56 MHz), Bluetooth (2.4 GHz), Wi-Fi (6 GHz), lowering potential risks of electromagnetic interference (EMI) in bodies. For example, magnetic resonance imaging (MRI) uses frequencies of MHz (20 MHz–300 MHz). The MRI compatibility of our optical communication system was evaluated by assessing its full communication capability, specifically, the successful optical transmission of messages through pig skin, under the external RF pulses (20 MHz). Additionally, MRI artifact testing was conducted with all wires removed, as full operational experiments within an MRI scanner could not be approved by external facilities due to safety management constraints. The experiments (Figure 2r) to see any interference during optical wireless communication in radio frequency (RF, 20 MHz) by the coil 1 clearly indicate that no observable interference is detected in the optical signals (blue line) when the RF (20 MHz, black line) is turned on at 3.5 s. More details are provided in the Experimental Section and Supplementary Video 1. We also demonstrated reliable optical message transmission through a pig skin under 20 MHz of RF pulses (Supplementary Video 2). In addition to the EMI, two other major factors that must be avoided for MRI compatibility are magnetic attractive force and induced electrical currents (eddy currents) in a rapidly changing strong magnetic field and RF pulse. To mitigate those effects, we used non-ferromagnetic conductive metals (titanium (Ti) and gold (Au)) in the circuit design, and implemented open-mesh structures in the ECG electrodes. More details of MRI compatibility test are provided in SI (Supplementary Fig. 6).

Uni-directional and bi-directional optical data transfer through biological tissues

Uni-directional data transfer through tissue can be achieved by integrating LEDs in the transmitter and a PD in the receiver to transmit information such as numbers or words as demonstrated in the experimental setup in **Figure 3a**. The transmitter (Tx, red box) facing to the skin emits light to deliver coded binary signals (Figure 3b) and the receiver (Rx, blue box) facing the skin detects the coded illumination (Figure 3c). As an example, the number '1' is transferred through the skin by sending ASCII-coded digital signals ('10001100', red in upper plot in Figure 3d) sequentially by turning on and off the LEDs. The lower plot (black) in Figure 3d shows the modulated signals detected by the Rx (PD). The received binary sequence ('10001100') is then decoded back to the number '1'. The bottom images are sequential ones to note each digit by on and off states. Similarly, more complex data, such as the word 'Alpha', can be transferred by sending all the alphabets coded in series, as shown in Figure 3e. More details are in the Experimental Section and Supplementary Videos 3 and 4.

With the integration of both the transmitter and receiver in one device (transceiver), bi-directional data transfer through biological tissue can be achieved as in Figure 3f. Requests and corresponding data can be wirelessly exchanged through the skin between two transceivers, to display the exchanged information on a serial monitor. As a demonstration of bi-directional data exchange, when a "Name" request is wirelessly transmitted (blue arrow) from the transceiver on the right through a biological tissue (Figure 3g), "Name : David" is wirelessly sent back (red arrow) to the transceiver, and displayed on the serial monitor. Additional data can be exchanged in a similar manner by sequentially requesting information such as "Age" (Figure 3h) and "Nationality" (Figure 3i). More details of the bi-directional optical data exchange are in the Experimental Section and Supplementary Video 5.

Demonstration of optical wireless data exchange for an implantable biomedical electronics

Bi-directional optical data exchange can be utilized to wirelessly retrieve information from an implanted electronic medical device upon requests from wearable electronics located outside of the body. To demonstrate the capabilities, we developed a flexible form of implantable sensing electronics, capable of recording electrocardiogram (ECG) and body temperature, integrated with the optical wireless transceiver as in **Figure 4a**. The fabricated implant including the ECG block (AD8232, Analog Devices), temperature sensing block, low-pass filter, microcontroller unit (MCU, ATtiny85, Atmel) and transceiver is shown in Figure 4b. The entire electronic implant is flexible enough to be bent over on a glass rod with a radius of 9 mm. A wearable electronics including the optical transceiver is also fabricated. The detailed designs of the medical implant are in SI (Supplementary Fig. 7).

To evaluate the performance of the optical wireless data transfer system *in vivo*, the fabricated electronic implant was inserted subcutaneously into a live mouse model (Figure 4d), while the wearable module was attached on the body (Figure 4e). Commercial ECG electrodes were attached to the legs for comparison. Figure 4f,g presents the real-time ECG and temperature signals (blue lines) acquired via optical wireless transfer to the wearable electronics. These wirelessly transferred signals are comparable to those obtained from commercial wired sensors (black lines). It should be noted that the body temperature remains constant because the measurements were from a live mouse model. To further validate the accuracy of the wireless temperature sensing, the external temperature sensor was subjected to controlled heating and cooling on a hot plate. The experimental setup is shown in SI (Supplementary Fig. 8). As shown in Figure 4h, the wirelessly acquired temperature signals (blue line) closely match those measured by a commercial wired thermocouple (black line).

The capability of bi-directional optical wireless communication is also demonstrated in more realistic scenarios in a live mouse model as shown with the experimental setup in Figure 4i. The flexible physiological sensors and wearable electronics with the built-in optical transceivers are implanted in and attached to the live mouse model to validate bi-directional communication. Data from the commercial ECG sensors and a thermometer are simultaneously monitored for comparison. More details of the experimental setup are in SI (Supplementary Fig. 9). Once a specific data type (① in Figure 4j) is selected, a corresponding request (② Tx: ECG or Temp.) is wirelessly transmitted to the implantable electronics (③ Rx: Data to collect). The implant then performs sensing (④) and signal processing (⑤). The collected data (⑥ Tx: ECG or Temp.) are subsequently transmitted back to the wearable electronics (⑦ Rx: Acquiring) wirelessly and displayed in real-time (⑧), demonstrating responsive bi-directional data exchange through biological tissue *in vivo*. More detailed data communication process for

ECG signal is provided in SI (Supplementary Fig. 10). The corresponding measurement results are plotted in Figure 4k. The physiological data such as ECG signals (blue lines) and temperature readings (red circles) are alternatively transmitted from inside the mouse model in response to specific requests from outside of the body. More details of the *in vivo* experiments are provided in the Experimental Section and Supplementary Video 6.

Discussion

Although we used pig skin as a proof-of-concept model whose compositions and optical properties are known to be similar to human skin, it does not capture the full variability of human skin pigmentation and optical properties across different populations. Such variations can significantly influence light transmission, absorption, and scattering, thereby affecting the efficiency and reliability of optical wireless data transfer in implantable devices. Future studies with human skin should include systematic evaluations across a range of human skin tones to establish performance boundaries and ensure the broad applicability of the proposed communication platform.

For the optical transceiver, we selected a light source with a peak wavelength of 670 nm because the measured optical transmittance (in **Figure 2e**) through pig skin (thickness: ~3 mm) was high enough (~20%) in wavelength greater than 600 nm when compared to the transmittance of 10% or less in lower wavelength (< 600 nm). It should be noted that infrared (IR) light with much higher wavelength can provide a benefit of deeper penetration through tissue and be more useful for deep implantation.

Our platform offers important advantages for enabling wireless communication in medical implants without potential disturbances, in a compact and flexible form. The optical transceivers operate without interference from other medical devices, such as MRI scanners, which may induce EMI or eddy currents, and it does not require coils or mechanical vibrations. Moreover, the device can be also realized in a very small and flexible form factor. In our lab, we successfully fabricated the ultrathin, submillimeter-scale transceivers using microLEDs (thickness: ~4 μm, each size: 250 × 250 μm^2) and photodetector (thickness: ~4 μm, size: 700 × 560 μm^2). These results suggest that further miniaturization and performance enhancement would be achievable in a dedicated fabrication facility. With these advantages, optical communication holds strong potential for safer and more comfortable implantable medical devices.

In summary, the results presented here demonstrate that the optical wireless data transfer system is capable of real-time, bi-directional data exchange through biological tissues by integrating microscale light-emitting diodes (LEDs) and photodetector (PD) into soft, flexible platforms. The optical approach without relying on traditional antenna coils, not only mitigates issues associated with EMI and eddy currents, may be very critical in MRI and other clinical settings, but also reduces the device footprint, the size of implants. Our systematic evaluation confirms the performance characteristics such as reliance on the distance, alignment, and tissue thickness between the optical transmitter and receiver. *In vivo* validation in live mouse models demonstrates that the optical transceiver, integrated with physiological sensors for electrocardiogram (ECG) and body temperature monitoring, along with a low-pass filter and microcontroller unit (MCU), enables real-time wireless signal acquisition and device control. The results highlight the potential of this platform for next-generation implantable medical devices, offering a safer and compact wireless communication in clinical and biomedical applications.

Methods

Preparation of the implantable optical wireless device

The implantable optical wireless device is fabricated through a double-sided (top-and-bottom) fabrication process. First, the bottom-side fabrication for ECG electrodes begins with a PI film (polyimide, ~25 μm) which was attached to a silicone layer (10:1 Polydimethylsiloxane (PDMS), ~10 μm, Sylgard184, Dow Corning, USA) coated on a slide glass. The ECG electrodes were formed by sputtering and wet chemical etching metal films (Ti/Au: 50 nm / 100 nm) on the PI film. Silver conductive epoxy (H20E, EPO-TEK Inc., USA) was dispensed onto the metal lines around the VIA (Vertical Interconnect Access) holes and thermally cured on a hot plate at 110 °C for 1 hour. Another PI layer (PI solution, ~2 μm) was spin-coated and cured to encapsulate the metal lines. The ECG electrodes were opened by reactive ion etching (RIE) with oxygen plasma. Second, the top-side fabrication for the optical wireless circuits begins with the RIE to form VIA holes for electrical connection between the bottom and top metal lines. The top layer circuits (Ti/Au: 50 nm / 100 nm) were sputtered and patterned by wet chemical etching. The silver conductive epoxy was dispensed onto the metal lines around the VIA (Vertical Interconnect Access) holes and thermally cured on a hot plate at 110 °C for 1 hour. The PI layer (PI solution, ~2 μm) was spin-coated and cured, followed by the RIE process to expose the LEDs and PD metal pad for cold-welding. The bottom contact metal films (Ti/Au: 10 nm / 100 nm) were deposited onto the bottom of the fabricated LEDs and PD attached on the stamp. To establish a direct bonding of the fabricated LEDs and PD onto the metal circuit, heat (95 °C) and pressure (~1.0 Mpa) were applied. After spin-coating and curing another PI layer (PI solution, ~2 μm), the RIE for opening top contact holes was processed. Interconnection line metal films (Ti/Au: 200 nm / 100 nm) were sputtered and patterned for electrical connection between the metal circuit and top contact metal of the LEDs and PD. The last PI layer (PI solution, ~2 μm) was spin-coated and cured, followed by the RIE process to expose the metal pads for connecting external wires. The PDMS was spin-coated onto the top layer for encapsulation.

Measurements of Electrical Properties of LEDs and PD

The current–voltage characteristics of the photodetector (PD) and the light-emitting diode (LEDs) were measured with a source measure unit (B2902A, Keysight Technologies). The performance of the LEDs was characterized by a sweep mode including off time (period: 200 ms, pulse width: 10 ms, duty cycle: 5%) between measurement points instead of a DC sweep mode to avoid a temperature rise from previous measurements. The performance of the PD was measured under red light illumination of the fabricated red LEDs (wavelength: 670 nm, optical power: 0.28 mW).

Measurements of Optical Properties

The external quantum efficiency (EQE) of the PD was measured in the wavelength range from 400 to 900 nm using a quantum efficiency measurement system (QuantX-300, Newport). Also, the electroluminescence (EL) spectrum of the LEDs was measured with an optical spectrometer (avaspec-ULS2048L, Avantes Corp.). The transmittance of the isolated pig skin (thickness: ~3 mm) was also measured with the optical spectrometer by collecting scattered light with doubleintegrating spheres.

Measurements of performance characteristics depending on distance and lateral misalignment

A custom-built motorized micro-stage (movement resolution: 0.1 μm) was used to adjust the distance and lateral misalignment between the transmitter and receiver. The receiver was fixed on a ground stage, and the transmitter was leveled and fixed on the movable micro-stage. The micro-stage was controlled to move from 0 to 50 mm in the longitudinal direction (distance control) and from 0 to 25 mm in the lateral direction (lateral misalignment control), respectively. An input voltage with a frequency of 1 Hz was applied to the transmitter, and the voltage generated at the receiver by the transferred light from the transmitter was measured.

Measurements of performance evaluation for the optical wireless data transfer under electromagnetic interference (EMI)

Two coils were used. One coil (Coil 1) was connected to a function generator to generate a 20 MHz RF pulse, and the other coil (Coil 2) was placed opposite the Coil 1 and connected to an oscilloscope to detect the induced interference. The optical wireless devices (transmitter and receiver) were positioned between two coils. The optically transferred signals of the receiver (PD) were measured during turning on/off the transmitter (LEDs, input voltage: 4 V, 1 Hz) before and after the induced RF pulses.

Uni-directional optical wireless data transfer through biological tissues

The transmitter was connected to a microcontroller board (Arduino Uno) to transmit ASCII-coded digital signals wirelessly to the receiver, which was connected to another microcontroller board. The received optical wireless signals at the receiver were decoded and displayed on the serial monitor on a laptop.

Bi-directional optical wireless data exchange through biological tissues

Two transceivers (A/B), each connected to a microcontroller board (Arduino Uno), were placed with an isolated pig skin positioned between them. Three buttons were connected to Transceiver A through the microcontroller board to transfer three types of questions to Transceiver B, which responded to the received questions. When Transceiver A sent a signal of "1", "2", or "3" as a question to Transceiver B, the Transceiver B responded by transmitting the corresponding data "Name : David", "Age : 32", or "Nationality : South Korea" back to the Transceiver A, respectively.

In vivo Experiments

The animal experiments were conducted by following the guidelines of Gwangju Institute of Science and Technology (GIST) Institutional Animal Care and Use Committee (GIST-2024-038) approval. Hairless mice (SKH1-Hrhr) were anesthetized by intraperitoneal injection of a mixture containing ketamine (50 mg/kg, Yuhan Ketamine 50, Yuhan), xylazine (5 mg/kg, Rompun Inj., Bayer Corp.,) and saline solution (Normal Saline Inj., Dae Han Pharm Co. Ltd.) with a total volume of 0.3 mL. The implantable electronics was inserted through an incision on the skin sterilized with a povidone iodine (povidone, Firson) and the wearable electronics was attached to a mouse model for optical wireless data exchange through biological tissues. Two buttons were connected to the wearable electronics through the microcontroller board to transfer two types of requesting, which were ECG and temperature of the mouse, to the implantable electronics. The wearable device transmitted signals "1" and "2" to request the corresponding data (ECG, Temp.) from the implantable device. In response, the implantable device transmitted the corresponding ECG or temperature data back to the wearable device and the transmitted signals were decoded and displayed on the serial monitor on a laptop. Regarding data rate, although the current system achieved ~1 kbps with simple on-off keying modulation, this speed is sufficient for bio-signal acquisition and device control. Moreover, the data rate can be further improved by shortening the pulse duration or implementing more advanced modulation schemes.

Data availability

Data supporting this study are provided within the manuscript or the supplementary information files.

Acknowledgements

This work was mainly supported by the National Research Foundation of Korea (NRF) grant funded by the Korea government (Ministry of Science and ICT, MIST) (No. RS-2023-00277831), and partially supported by the GIST-MIT Research Collaboration grant funded by the GIST. English writing was corrected by using an online tool.

Author contributions

J.L. planned and supervised the concept. C.H. fabricated the device, and performed measurements of electrical and optical characteristics supported by T.L. T.L. provided advice and discussion on the concept. D.J. provided advice and discussion on the chip bonding process. C.H., D.J. performed the animal surgeries. J.L. and C.H. wrote the manuscript. All authors read and commented on the manuscript.

Competing interests

The authors declare no competing financial interests.

Additional information

Supplementary information is available online.

References

1 Li, Y. *et al.* Molecular mechanisms of aging and anti-aging strategies. *Cell Communication and Signaling* **22**, 285 (2024).

2 Guo, J. *et al.* Aging and aging-related diseases: from molecular mechanisms to interventions and treatments. *Signal transduction and targeted therapy* **7**, 391 (2022).

3 Niccoli, T. & Partridge, L. Ageing as a risk factor for disease. *Current biology* **22**, R741–R752 (2012).

4 Ouyang, H. *et al.* Symbiotic cardiac pacemaker. *Nature communications* **10**, 1821 (2019).

5 Choi, Y. S. *et al.* Fully implantable and bioresorbable cardiac pacemakers without leads or batteries. *Nature biotechnology* **39**, 1228–1238 (2021).

6 Lee, G. *et al.* A bioresorbable peripheral nerve stimulator for electronic pain block. *Science advances* **8**, eabp9169 (2022).

7 Koo, J. *et al.* Wireless bioresorbable electronic system enables sustained nonpharmacological neuroregenerative therapy. *Nature medicine* **24**, 1830–1836 (2018).

8 Cai, Y. *et al.* In-situ artificial retina with all-in-one reconfigurable photomemristor networks. *npj Flexible Electronics* **7**, 29 (2023).

9 Lan, L. *et al.* Stretchable optoelectronic synapses with ultraviolet to near-infrared perception for retina-inspired computing and vision-adaptive sensing. *npj Flexible Electronics* **9**, 16 (2025).

10 Zeng, F.-G., Rebscher, S., Harrison, W., Sun, X. & Feng, H. Cochlear implants: system design, integration, and evaluation. *IEEE reviews in biomedical engineering* **1**, 115–142 (2008).

11 Dhanasingh, A. & Jolly, C. An overview of cochlear implant electrode array designs. *Hearing research* **356**, 93–103 (2017).

12 Qiu, S., Yan, B. P. & Zhao, N. Stroke-volume-allocation model enabling wearable sensors for vascular age and cardiovascular disease assessment. *npj Flexible Electronics* **8**, 24 (2024).

13 Bhattacharya, S. *et al.* A chest-conformable, wireless electro-mechanical e-tattoo for measuring multiple cardiac time intervals. *Advanced Electronic Materials* **9**, 2201284 (2023).

14 Burton, A. *et al.* Fully implanted battery-free high power platform for chronic spinal and muscular functional electrical stimulation. *Nature communications* **14**, 7887 (2023).

15 Mahmood, M. *et al.* Wireless Soft Scalp Electronics and Virtual Reality System for Motor Imagery-Based Brain–Machine Interfaces. *Advanced Science* **8**, 2101129 (2021).

16 Zhu, G. *et al.* Neural stimulation and modulation with sub-cellular precision by optomechanical bio-dart. *Light: Science & Applications* **13**, 258 (2024).

17 La, T. G. *et al.* Two-layered and stretchable e-textile patches for wearable healthcare

electronics. *Advanced healthcare materials* **7**, 1801033 (2018).

18 Cho, Y., Park, S., Lee, J. & Yu, K. J. Emerging materials and technologies with applications in flexible neural implants: a comprehensive review of current issues with neural devices. *Advanced Materials* **33**, 2005786 (2021).

19 Jiang, L. *et al.* Flexible ultrasound-induced retinal stimulating piezo-arrays for biomimetic visual prostheses. *Nature communications* **13**, 3853 (2022).

20 Zheng, T., Xie, X., Shi, Q., Wu, J. & Yu, C. Self-Powered Artificial Neuron Devices: Towards the All-In-One Perception and Computation System. *Advanced Materials* **37**, 2416897 (2025).

21 Xu, B. *et al.* An epidermal stimulation and sensing platform for sensorimotor prosthetic control, management of lower back exertion, and electrical muscle activation. *Advanced Materials (Deerfield Beach, Fla.)* **28**, 4462 (2015).

22 Kim, D. *et al.* Hexagonal metal complex based mechanically robust transparent ultrathin gold μECoG for electro-optical neural interfaces. *npj Flexible Electronics* **9**, 31 (2025).

23 Kim, A., Ochoa, M., Rahimi, R. & Ziaie, B. New and emerging energy sources for implantable wireless microdevices. *IEEE access* **3**, 89–98 (2015).

24 Kurs, A. *et al.* Wireless power transfer via strongly coupled magnetic resonances. *science* **317**, 83–86 (2007).

25 Li, P. & Bashirullah, R. A wireless power interface for rechargeable battery operated medical implants. *IEEE Transactions on Circuits and Systems II: Express Briefs* **54**, 912–916 (2007).

26 Choi, Y. S. *et al.* A transient, closed-loop network of wireless, body-integrated devices for autonomous electrotherapy. *Science* **376**, 1006–1012 (2022).

27 Kim, C. Y. *et al.* Soft subdermal implant capable of wireless battery charging and programmable controls for applications in optogenetics. *Nature communications* **12**, 535 (2021).

28 Kim, D.-H. *et al.* Epidermal electronics. *science* **333**, 838–843 (2011).

29 Shao, Y. *et al.* Room-temperature high-precision printing of flexible wireless electronics based on MXene inks. *Nature communications* **13**, 3223 (2022).

30 Boutry, C. M. *et al.* Biodegradable and flexible arterial-pulse sensor for the wireless monitoring of blood flow. *Nature biomedical engineering* **3**, 47–57 (2019).

31 Kim, J. *et al.* Miniaturized flexible electronic systems with wireless power and near-field communication capabilities. *Advanced Functional Materials* **25**, 4761–4767 (2015).

32 Lee, A.-H., Lee, J., Leung, V., Larson, L. & Nurmikko, A. Patterned electrical brain stimulation by a wireless network of implantable microdevices. *Nature Communications* **15**, 10093 (2024).

33 Bathaei, M. J. *et al.* Photolithography-based microfabrication of biodegradable flexible and

stretchable sensors. *Advanced Materials* **35**, 2207081 (2023).

34 Lu, X., Wang, P., Niyato, D., Kim, D. I. & Han, Z. Wireless charging technologies: Fundamentals, standards, and network applications. *IEEE communications surveys & tutorials* **18**, 1413–1452 (2015).

35 Chandrakasan, A. P., Verma, N. & Daly, D. C. Ultralow-power electronics for biomedical applications. *Annu. Rev. Biomed. Eng.* **10**, 247–274 (2008).

36 Haerinia, M. & Shadid, R. Wireless power transfer approaches for medical implants: A review. *Signals* **1**, 209–229 (2020).

37 Kim, K. Y. *et al.* An ultrathin organic–inorganic integrated device for optical biomarker monitoring. *Nature Electronics* **7**, 914–923 (2024).

38 Cortese, A. J. *et al.* Microscopic sensors using optical wireless integrated circuits. *Proceedings of the National Academy of Sciences* **117**, 9173–9179 (2020).

39 Zhang, H. *et al.* Wireless, battery-free optoelectronic systems as subdermal implants for local tissue oximetry. *Science advances* **5**, eaaw0873 (2019).

40 Burton, A. *et al.* Wireless, battery-free subdermally implantable photometry systems for chronic recording of neural dynamics. *Proceedings of the National Academy of Sciences* **117**, 2835–2845 (2020).

41 He, H. *et al.* Integrated sensing and communication in an optical fibre. *Light: Science & Applications* **12**, 25 (2023).

42 Jacobi, U. *et al.* Porcine ear skin: an in vitro model for human skin. *Skin Research and Technology* **13**, 19–24 (2007).

43 TP, S. The pig as a model for human wound healing. *Wound Rep Reg* **91**, 66–76 (2001).

44 Summerfield, A., Meurens, F. & Ricklin, M. E. The immunology of the porcine skin and its value as a model for human skin. *Molecular immunology* **66**, 14–21 (2015).

45 Lee, Y. & Hwang, K. Skin thickness of Korean adults. *Surgical and radiologic anatomy* **24**, 183 (2002).

CAPTION

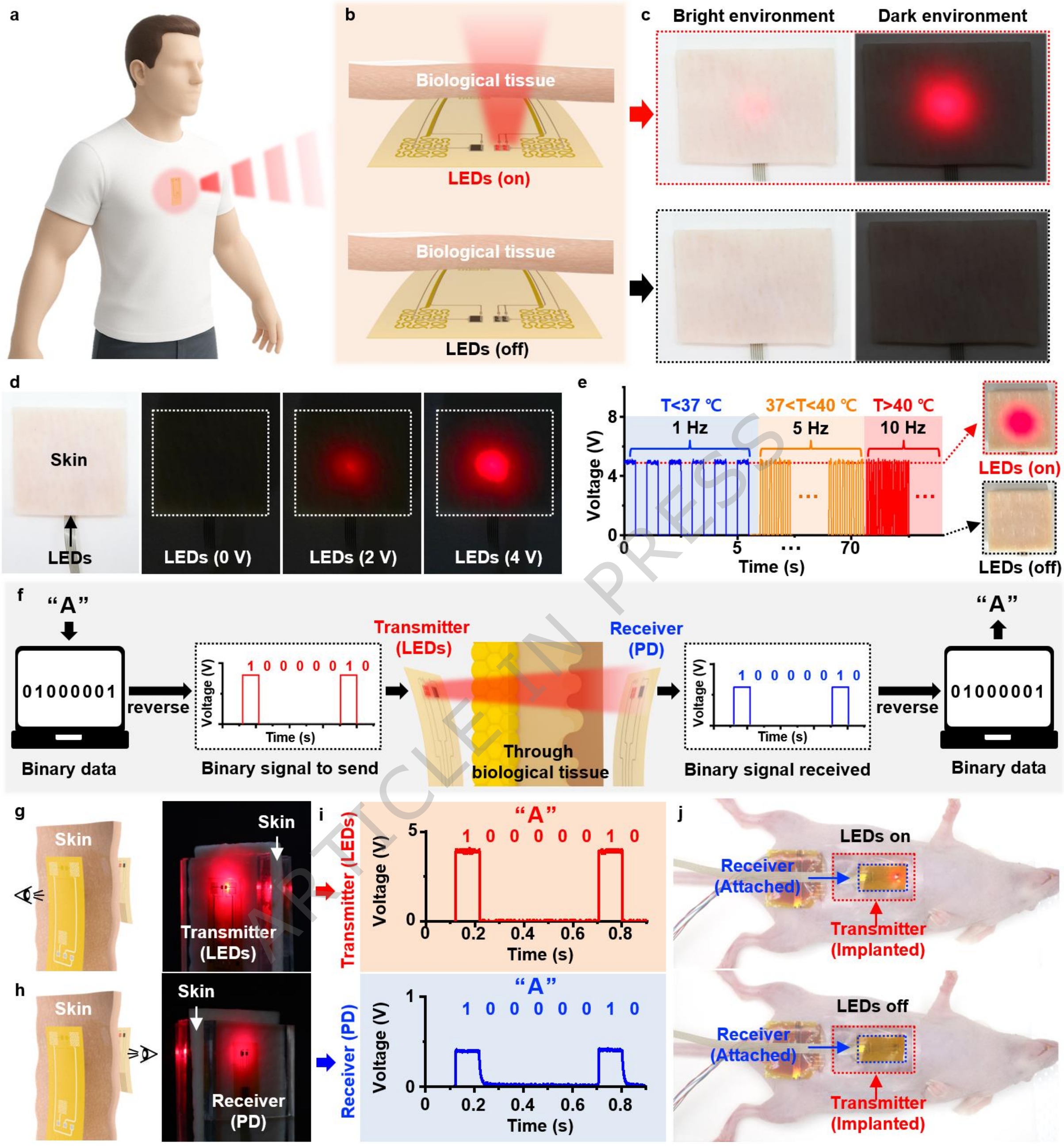

Figure 1. Optical wireless data transfer through biological tissues. a. Conceptual illustration of the optical wireless data transfer from a body. **b.** Illustrations of signaling from an implanted device (LEDs) through skin tissue with the LEDs on (top) and off (bottom). **c.** Optical images of the outer skin with the implanted LEDs on (top) and off (bottom). **d-e.** Data

transfer based on magnitudes of the signals (d) in brightness and (e) frequency. **f.** Data transfer by converting the alphabet ‘A’ to binary data and generating the binary signals to send through biological tissue by blinking to note the binary digit ‘0’ and ‘1’. The binary signals are captured by a photodetector (PD), followed by converting back to the original alphabet ‘A’. **g-h.** Illustrations and optical images of the optical wireless communication through an isolated pig skin (thickness, *t*: ~3 mm) placed between the optical signal (g) transmitter (LEDs) and (h) receiver (photodetector, PD). **i.** Applied input signals (top) to the transmitter (LEDs) and corresponding measured signals (bottom) through the skin to the receiver (PD). **j.** Photograph of a mouse model with the implanted signal transmitter and attached signal receiver.

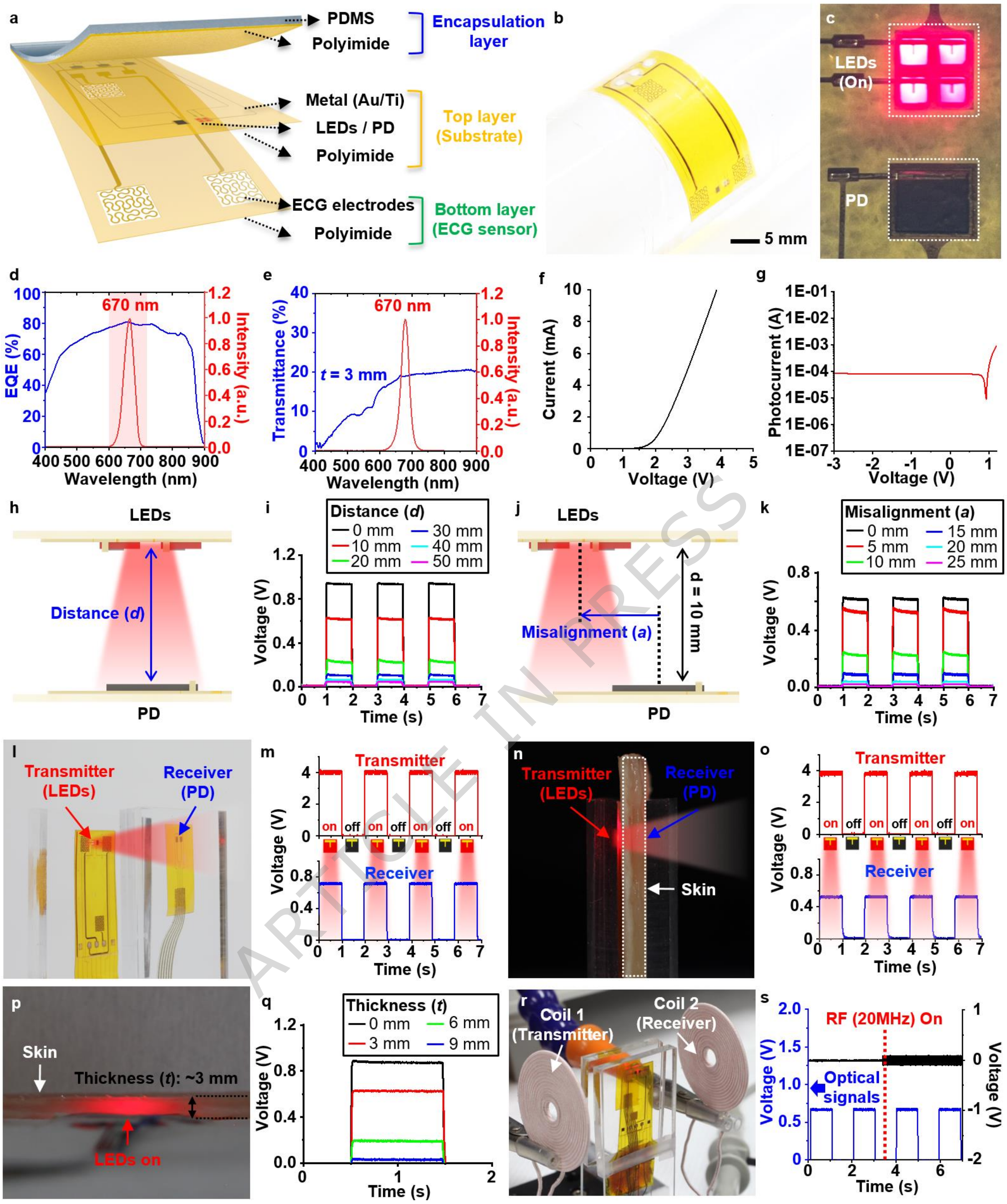

Figure 2. Design and performance characteristics of the implantable optical wireless device. a. Exploded view of the device including a custom-made ultra-thin inorganic LEDs (AlGaInP) and PD (GaAs) as a bi-directional optical wireless transceiver, and electrocardiogram (ECG) electrodes as a biological sensor. **b.** Optical image of the fabricated

device wrapped on a glass rod with a bending radius of 9 mm. **c.** Magnified optical image of the fabricated LEDs (2 × 2 array, each size: 250 × 250 μm^2, thickness: ~4 μm) and the PD (size: 700 × 560 μm^2, thickness: ~4 μm). **d.** Measured external quantum efficiency (EQE) of the PD (blue line) and electroluminescence (EL) spectrum of the LEDs (red line). **e.** Optical transmittance (blue line) of the light (~670 nm) from the LEDs through an isolated pig skin (thickness, *t*: 3 mm), which has compositions and optical properties similar to human skin. EL spectrum of the LEDs is in red line. **f-g.** Current–voltage characteristics of the (f) LED and (g) PD under red light illumination (wavelength 670 nm, optical power 0.28 mW). **h-k.** Performance characteristics depending on (h) distance (*d*) and (j) lateral misalignment (*a*) between the LEDs and PD. The measured voltages by PD are reduced down to 45 mV at the longer (i) distance (50 mm) or down to 24 mV by (k) misalignment (25 mm) but the signals are still detectable. **l-o.** Experimental setups and measurement results of optical wireless data transfer (l,m) directly from the LEDs to PD (distance: 3 mm) and (n,o) through biological tissue (pig skin, thickness: 3 mm). **p.** Cross-sectional view of the pig skin (thickness, *t*: ~3 mm) showing light penetration with the LEDs on. **q.** Measurement results of the detected voltage from the receiver PD, depending on the skin thickness (t = 0−9 mm). Transmitter (LEDs) input voltage: 4 V. **r.** Optical image of the experimental setup to evaluate the performance of the optical wireless communication under electromagnetic interference (EMI) caused by the radio frequency from the coil 1 at 20 MHz. Coil 2 detects induced interference. **s.** Optically transferred signals (blue pulses) measured by the receiver (PD) before and after the RF pulses (black line) are induced. No disturbance is detected, attributed to the frequency difference between visible light and radio-frequency signals.

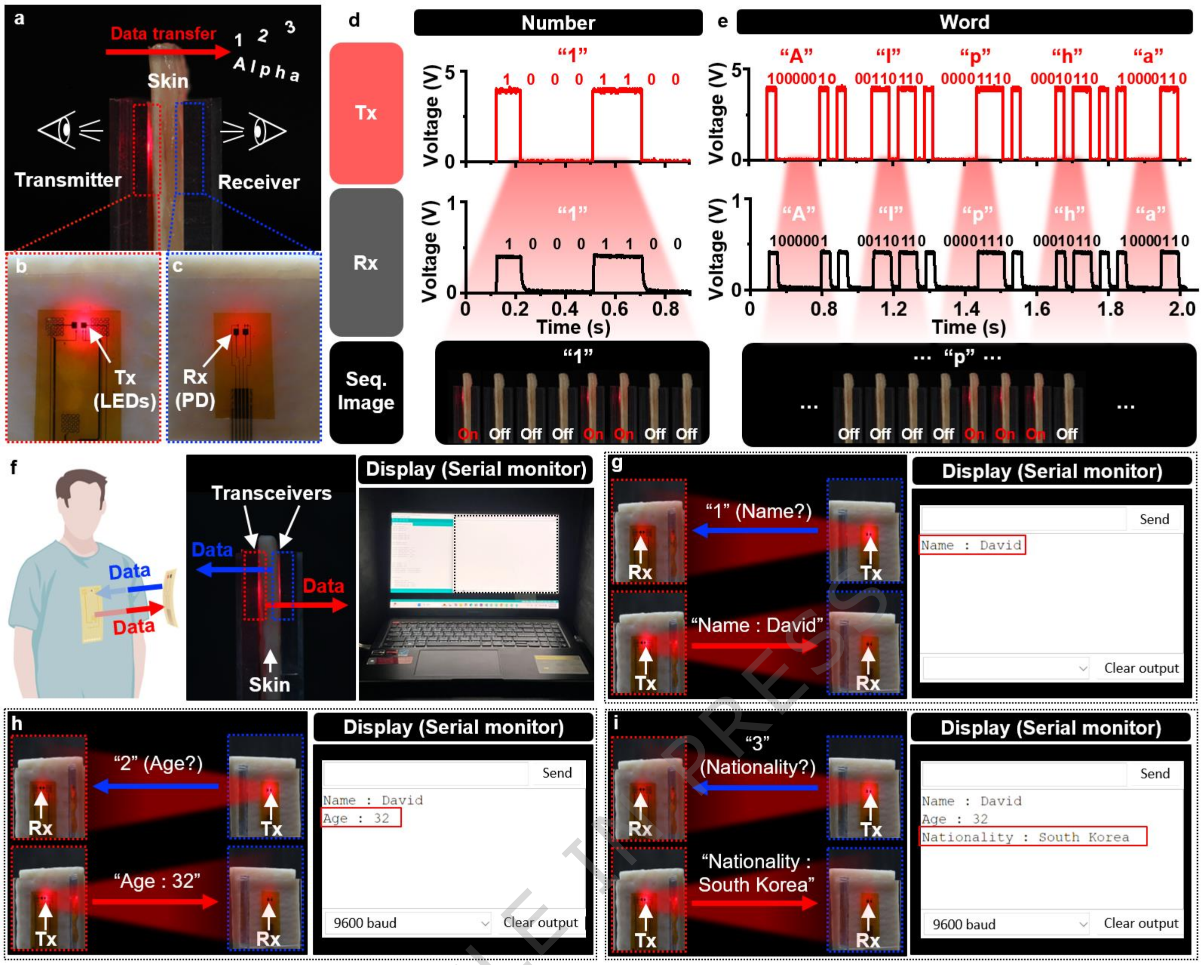

Figure 3. Uni-directional and bi-directional optical data transfer through biological tissues. a. Uni-directional optical wireless data transmission through an isolated pig skin interposed between the transmitter (Tx, red box) and receiver (Rx, blue box). **b.** Transmitter facing to the skin with the LEDs on. **c.** Receiver facing to the skin to detect penetrated light through the skin. **d.** Uni-directional wireless data transmission of a number '1'. The transmitter generates the ASCII-coded digital signals ('10001100') sequentially by turning on/off state of the LEDs to transfer through the skin. The PD in the receiver reads the signals ('10001100') through the skin. The transmitted signals are decoded to '1'. The bottom images are sequential ones to note each digit by on and off states. **e.** Uni-directional wireless data transmission of a word 'Alpha'. All the alphabets are coded to binary digits and transmitted to the receiver

through the skin. **f.** Demonstration of bi-directional optical wireless data transmission through an isolated pig skin. Data can be sent back and forth between two transceivers to display on a serial monitor (patient illustration created with BioRender.com). **g.** Bi-directional wireless data transfer to ask a name (coded to ‘1’) in one direction (blue arrow) and answer with ‘David’ to the other direction (red arrow). The name is displayed on a monitor. **h-i.** Additional data can be sequentially exchanged through the skin to ask and answer (h) age and (i) nationality.

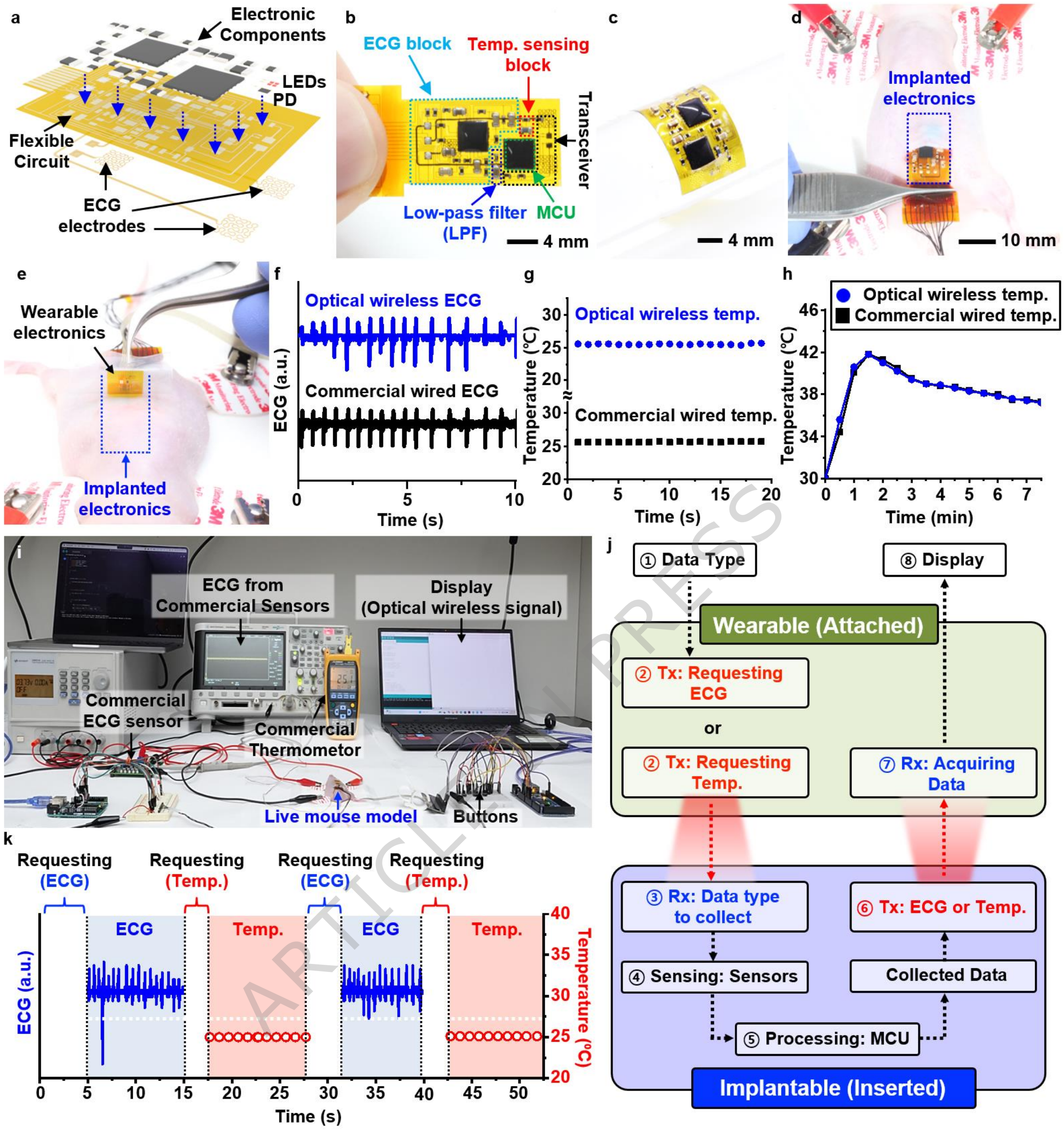

Figure 4. Demonstration of optical wireless data exchange for an implantable biomedical electronics. a. Integration of the implantable optical wireless units (transceiver) along with electronic components on a flexible substrate for sensing and processing. **b.** Fabricated implantable electronics that can process and send out in-body ECG and temperature signals upon request from out of a body. **c.** Optical image of the flexible electronic implant with a function of optical wireless bi-directional communication, wrapped on a glass rod with a

bending radius of 9 mm. **d-e.** Optical images of (d) the implantable electronics and (e) wearable electronics inserted in and attached to a mouse model, respectively. Commercial ECG electrodes are attached for comparison. **f-g.** Acquired real-time (f) ECG and (g) temperature signals (blue) wirelessly-transferred to the wearable electronics while being measured in the implanted electronics. The transferred signals are comparable with the results from a commercial wired sensor (black). **h.** Measurement results of wirelessly acquired real-time temperature (blue dots) from the implantable electronics on a hot plate to intentionally change temperature. The wirelessly acquired temperatures are comparable with the measurements from a commercial wired thermocouple (black dots). **i.** Experimental setup for bi-directional optical wireless communication in a live mouse model. **j.** Flow chart of multi-modes measurements and bi-directional wireless communication with the wearable and implantable electronics in a mouse model. **k.** Measurement results of the internal biological data (ECG, temperature) from inside the body upon sequentially requesting from outside the body via bi-directional optical wireless data exchange.